Impact of tool rotational speed on friction stir welded joints of AA2014-T6/AA5052-H32: synthesis, microstructural, mechanical and fractographic behaviour

Sathya Narayana N, Mervin A. Herbert, Arun Kumar Shettigar
Department of Mechanical Engineering, NITK, Surathkal, Mangaluru – 575025, India
sathyazen2@gmail.com, http://orcid.org/0000-0001-2345-6789
merhertoma@nitk.edu.in, akshettigar@nitk.edu.in

Manjunath Vatnalmath
Department of Mechanical Engineering, RNS Institute of Technology, Bengaluru-560098, Visvesvaraya Technological University Karnataka, India
vmanjunathsit@gmail.com, https://orcid.org/0000-0003-3138-9453

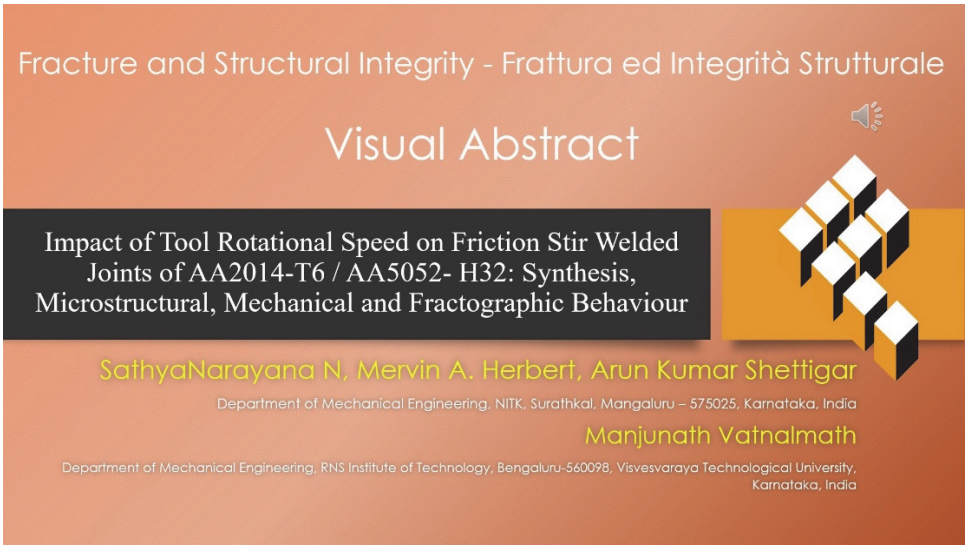

Citation: Sathya, N. N., Herbert, M. A., Shettigar, A. K., Vatnalmath, M., Impact of tool rotational speed on friction stir welded joints of AA2014-T6/AA5052-H32: synthesis, microstructural, mechanical and fractographic behaviour, Fracture and Structural Integrity, 75 (2026) 1-12.

Received: 06.08.2025
Accepted: 30.09.2025
Published: 11.10.2025
Issue: 01.2026

KEYWORDS. FSW, Tool rotation speed, UTS, Yield strength, Vickers hardness, Fractography

INTRODUCTION

Friction stir welding (FSW) has emerged as an important solid-state joining technique, particularly for aluminium alloys, which are widely recognized for their high strength-to-weight ratio, corrosion resistance, and formability [1]. Unlike conventional fusion welding, FSW operates well beneath the melting point of the base materials, utilizing the rotating, non-consumable tool to induce severe plastic deformation and localized heating at the joint interface [2]. This process engenders a dynamically recrystallized microstructure, resulting in welds with enhanced mechanical properties and minimal distortion [3]. The significance of FSW in relation to the aluminium alloys is multifaceted. Traditional fusion welding

methods often result in deleterious defects, such as porosity, hot cracking, and significant residual stresses, particularly in high-strength alloys, including the 2xxx and 7xxx series [4]. FSW, by circumventing the liquid phase, obviates these issues and produces joints with superior tensile strength, ductility, and fatigue performance [5]. Furthermore, the process is energy-efficient, environmentally benign, and does not necessitate consumables such as filler metals or shielding gases, thus aligning sustainable manufacturing paradigms [6]. FSW has been ubiquitously adopted in critical sectors. In aerospace, it plays a crucial role in the fabrication of lightweight, high-integrity structures, such as aircraft fuselage panels and rocket fuel tanks, where weld reliability is paramount. FSW has been ubiquitously adopted in critical sectors. The automotive industry exploits FSW to produce crash-resistant components and battery enclosures, leveraging the process's ability to yield joints with minimal distortion and high repeatability. In shipbuilding and rail transport, FSW enables the assembly of large aluminium panels with excellent dimensional stability and corrosion resistance. [7-8].

The FSW process relies on precise control of tool rotation speed, welding speed, tool geometry, and axial force to regulate thermomechanical conditions that govern joint quality. These parameters synergistically influence heat generation patterns, plasticized material flow dynamics, and microstructural transformations in aluminium alloys. Thilagham et al. [9] investigated friction stir welding of AA5052-H2 and AA6082-T6 aluminium alloys, analyzing tilt angle (2°), travel speed (60–120 mm/min), and rotational speed (600–1200 rpm) effects on joint microstructure and mechanical performance. Optimized parameters yielded a peak nugget zone hardness of HV115 and 56% joint efficiency, with tensile strength, elongation, yield load, and yield stress demonstrating parameter-dependent enhancements. The findings highlighted the critical influence of process variables on weld integrity and property gradation in dissimilar aluminium alloy joints. Tool rotation speed (TRS) directly governs frictional heating at the tool-workpiece interface. Li et al. [10] observed that, at higher rotational speeds, the nugget zone develops an onion ring morphology due to dynamic recrystallization, producing fine equiaxed crystals. However, excessive speeds lead to larger grain sizes, which diminishes the strengthening effect of grain boundaries. According to Sanjeev Kumar et al. [11], excessive tool TRS above 1400 rpm in AA2050-T84 welds caused flash formation and reduced hardness by 12% due to precipitate dissolution. Higher tool speed also causes the coarsening of grains in aluminium alloys. The moderate increase in TRS (800–1200 rpm) enhances dynamic recrystallization, producing finer grains (7–9 μm) in the nugget zone (NZ) and improving tensile strength due to controlled heat input and plastic deformation. However, excessive speeds (above 1200 rpm) generate excessive frictional heat, causing grain coarsening (up to 15 μm), dissolving strengthening precipitates, and reducing hardness by 12–18% [12]. There are numerous studies that have attempted the FSW on dissimilar aluminium alloys. However, the FSW on aluminium alloys AA2014-T6 and AA5052-H32 is critically found. The importance of joining AA2014-T6 and AA5052-H32 aluminium alloys in aerospace and automobile applications lies in their complementary properties, which enable the creation of lightweight, high-performance components optimized for both structural integrity and environmental resistance. AA2014-T6, a high-strength copper-based alloy, is favored in aerospace for critical load-bearing structures due to its exceptional strength-to-weight ratio and fatigue resistance. In contrast, AA5052-H32, a magnesium-rich alloy, offers superior corrosion resistance and formability, making it ideal for automotive body panels, fuel tanks, and marine-grade components. The present study aimed at producing FSW joints of these dissimilar aluminium alloys by varying the tool speed (860-1460 RPM) while keeping the feed rate or welding speed constant at 40 mm/min to investigate the effect of TRS on the weld microstructure and strength.

MATERIALS AND METHODS

Aluminium plates of AA2014-T6 and AA5052-H32, with a geometrical thickness of 6 mm, are selected as base metals. Tab. 1 shows the chemical composition of base metals. The base metals are prepared to a dimension of 150 x 50 mm² using a wire-cut electric discharge machine (EDM) to facilitate the FSW process. Tab. 2 shows the mechanical properties of the base metals. The tool, made of H13 steel with a cylindrical pin profile featuring an 18 mm shoulder, a 5.7 mm pin length, and a 6 mm pin diameter, is used in the present study. The chemical composition of the tool used is illustrated in Tab. 3.

Material	Cu	Mn	Si	Mg	Fe	Zn	Ti	Cr	Ni	Al
AA2014-T6	4.50	0.84	0.70	0.60	0.25	0.09	0.02	0.01	0.01	92.98
AA5052-H32	0.04	0.07	0.07	2.45	0.35	0.03	0.02	0.20	0.01	96.76

Table 1: Elemental composition of base metals in wt.%.

Material	0.2% Yield stress (MPa)	UTS (MPa)	Elongation (%)	Hardness (HV)
AA2014-T6	453	468	14	162
AA5052-H32	182	225	15	78

Table 2: Mechanical properties of base materials.

Cr	Mo	Si	V	C	Cu	Ni	Mn	S	P	Fe
4.48	1.22	0.86	0.84	0.32	.30	0.30	0.20	0.03	0.03	91.42

Table 3: Chemical composition of Tool H13 in wt.%.

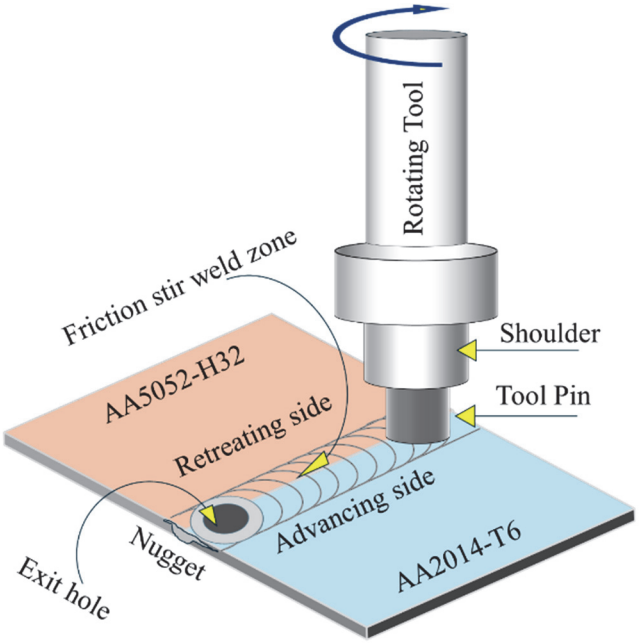

Figure 1: Schematic illustration of the FSW process

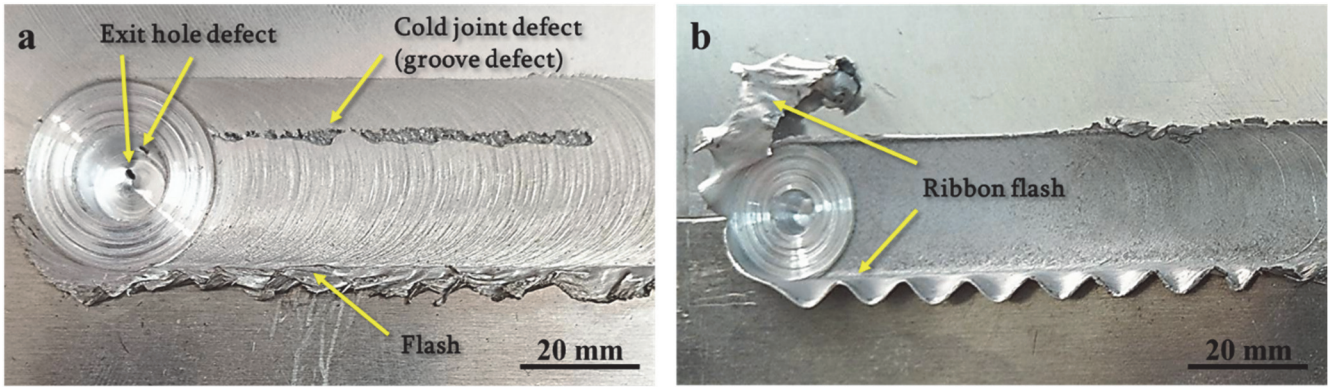

Figure 2: Visual defects at the FSW joints made at a) 760 rpm b) 1560 rpm

FSW process

The plates were meticulously cleaned with acetone to eliminate any surface contaminants and foreign particles. FSW is performed in a butt joint configuration using a CNC 4-axis FSW machine with different TRS of 860-1460 rpm. Fig. 1 demonstrates a schematic illustration of the current FSW process. For the welding setup, the AA2014-T6 alloy, owing to its superior hardness relative to AA2014-T6, is positioned on the advancing side (AS), while AA5052-H32 is placed on the retreating side (RS). This arrangement is known to promote elevated temperature and heat generation in the weld zone. The

TRS range is chosen based on the various trial experiments. The FSW joints made at TRS of 760 and 1560 rpm showed colossal defects at the weld surface. Fig. 2 (a, b) shows visual defects at the FSW joints made at 760 and 1560 rpm. Throughout the process, the tool tilt angle and welding speed are maintained constant at 1° and 40 mm/min, respectively. The higher hardness of AA2014-T6 on the advancing side is anticipated to induce increased shearing action and frictional heat during the welding process, thereby influencing the thermal profile and material flow characteristics of the joint [13]. The tool is rotated in the anticlockwise direction during welding. As the tool rotates, it exerts pressure on the material along the butt joint line, following the direction of rotation while simultaneously applying a downward force. The frictional heat generated by this motion softens the material, enabling it to flow inward and consolidate effectively within the joint. This controlled material flow and plasticization result in a robust weld with enhanced joint strength [11].

Weld morphology analysis

The welded specimens for microstructural examination are cut at right angles to the welding trajectory, measuring 20 mm × 10 mm. The prepared samples are polished with 320 to 2000 grit silicon carbide (SiC) papers, followed by final cloth polishing using 0.25–0.5 µm diamond suspension to achieve a mirror-like finish. Etching is performed using Keller's reagent to reveal the microstructural features. Detailed characterization of the welded joints and base materials is conducted by using optical microscopy (OM) and scanning electron microscopy (SEM) to examine various zones such as heat-affected zone (HAZ), stir zone (SZ), and thermomechanical affected zone (TMAZ). Tensile testing is performed to evaluate the mechanical properties of the welds. The grain size measurement was done according to ASTM E112/E1382-91 (Heyns Lineal Interception) standard by Infinity microscopes and optics-V6.1 (K-Metallurgy Pro). Tensile specimens are prepared according to the ASTM E8/E8M (2016) standard [15], with the tensile axis oriented orthogonally to the welding direction. The tensile test is conducted using a computer-integrated universal testing machine with a 10 kN capacity, at a strain rate of 0.5 mm/min and ambient temperature. For each welding condition, three tensile specimens are tested. The fractured surfaces of the tensile specimens are analyzed for ductile and brittle failure features using SEM. Vickers microhardness measurements are conducted to assess the hardness profile across the weld cross-section. Indentations are made at a depth of 3 mm from the top surface of the weld, along a 25 mm length, with 1.5 mm spacing between indentations. A load of 100 g is applied for a dwell time of 10 seconds, in accordance with ASTM E384-10.

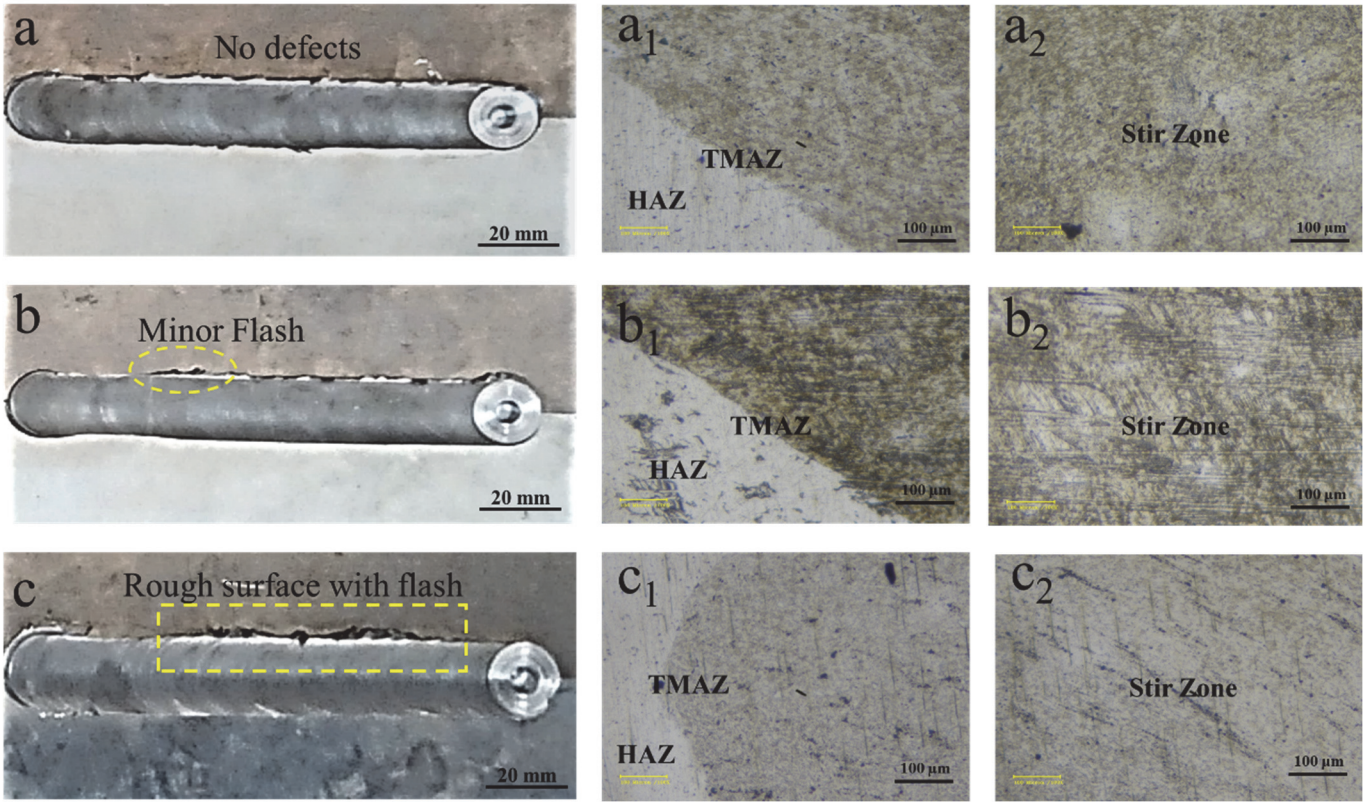

Figure 3: Macro images of FSW joints, a) 860 rpm, b) 1160 rpm, and c) 1460 rpm, and (a1-c2) respective optical micrographs

RESULTS AND DISCUSSION

Microstructure

The optical micrographs shown in Fig. 3 (a-c) demonstrate the critical influence of tool rotational speed on weld quality, revealing distinct microstructural zones and progressive defect formation as rotational speed increases from 860 to 1460 rpm. At 860 rpm, the optimal heat input produces defect-free welds with clearly defined zones (Fig.3 a_1), including the stir zone (Fig.3 a_2) characterized by equiaxed recrystallized grains due to continuous recrystallization, the TMAZ showing significant elongated grains, and HAZ exhibiting thermal effects without plastic deformation. As the rotational speed increases to 1160 rpm (Fig.3 b), excessive heat generation begins to compromise the weld quality, leading to minor flash formation due to over-plasticization of material and inadequate consolidation beneath the tool shoulder. At the highest speed of 1460 rpm (Fig. 3 c), severe defects manifest rough surfaces with significant flash, attributed to excessive frictional heat, causing abnormal material flow and ejection from the weld zone. Excessive rotational speeds generate excessive heat input, leading to the formation of flash defects, rough surfaces, and potential cavity formation due to inadequate stirring, while optimal speeds produce defect-free joints with proper grain refinement [14]. The microstructural evolution follows established mechanisms where continuous dynamic recrystallization occurs in the nugget zone through dislocation-glide-assisted sub-grain rotation, resulting in high-misorientation boundaries and fine grain depending on processing parameters [15]. The asymmetric nature of the zones, particularly the difference between advancing and retreating sides in terms of precipitate distribution and hardness, reflects the complex thermo-mechanical process during FSW, with studies showing that optimized rotational speeds maintain fine precipitate structures essential for mechanical property retention [16]. Optimized TRS and defect-free weld surface are also attributed to the base metal properties. The distinct zones are observed in the SEM images: the HAZ, TMAZ, and SZ, each of which exhibits different microstructural characteristics depending on the rotational speed employed. Fig. 4 (a-d) shows the SEM images of the FSW joint made at TRS of 860 rpm. Fig. 4 (a and d) shows the SEM images of base metals AA5052-H32 and AA2014-T6, respectively. Fig. 4 (c) shows the distinct HAZ and TMAZ zones. The HAZ exhibits minimal microstructural degradation, characterized by controlled grain coarsening and limited precipitate dissolution. The TMAZ exhibits well-controlled deformation characteristics with elongated grains showing evidence of material flow around the tool without excessive thermal damage. TMAZ experiences both thermal and mechanical effects, with temperatures lower than the stir zone but sufficient plastic deformation to alter grain morphology. The controlled thermal conditions at TRS, with a speed of 860 rpm, maintain the desired balance between mechanical deformation and thermal exposure. Further, when the TRS increased to 1160 rpm, the TMAZ (Fig. 4 f) shows more thermal effects with increased grain coarsening and greater precipitate dissolution compared to the TRS of 860 rpm. The TMAZ at the TRS of 1460 rpm (Fig. 4 j) shows severe thermal overexposure leading to uncontrolled microstructural changes and loss of the desired deformation characteristics. The excessive heat input creates conditions in which grain boundary migration occurs without the stabilizing influence of controlled deformation. It significantly disrupts the material flow patterns, causing chaotic flow and inadequate consolidation, with potential void formation. The central zone of the weld area, known as the SZ, undergoes substantial deformation due to the rotating tool pin, resulting in severe stirring action that heats this area and leads to plastic deformation of the material. The SZ of FSW joint made at TRS of 860 rpm (Fig. 4 c) shows fine, equiaxed grains. The absence of voids and cracks indicates the uniformity of microstructure and adequate material mixing. However, the SZ at high TRS of 1160 (Fig. 4 g) and 1460 rpm (Fig. 4 k) shows the microstructural degradation with grain coarsening and reduced recrystallization efficiency. The voids and cracks visible confirm the formation of welding defects due to over-softening and poor joints [5]. The average grain size of SZ is measured using optical micrographs to confirm the coarsening of grains with an increase in the TRS. Fig. 5 shows variations in SZ grain size at various TRS. It shows a progressive increase in grain size from approximately 11.8 ± 0.3 μm at 860 RPM to 15.7 μm at 1460 RPM. The increasing grain size with higher tool rotation speeds observed in the graph is fundamentally attributed to the elevated heat generated during the FSW process. Moreover, the heat generation rate is influenced by the TRS, and the peak temperature decreases as the tool rotational speed decreases. The grain size increases with an increase in the peak temperature, mainly due to the increased TRS [17]. Fig. 6 (a-e) presents the SEM image along with the corresponding EDS elemental mapping of aluminum (Al), magnesium (Mg), and copper (Cu) on the retreating side of the FSW joint, which was fabricated at a tool rotational speed (TRS) of 860 rpm. The elemental mapping reveals distinct distribution patterns for each component in the friction stir welded joint produced at TRS of 860 rpm. Aluminium (97.19 at%) exhibits uniform distribution throughout the analyzed region, indicating adequate material mixing and successful stirring action achieved by the optimal rotational speed that creates sufficient heat input and material flow for homogeneous redistribution of the base matrix material. The magnesium (2.29 at%) appears to be predominantly distributed towards the AA5052-H32 side. However, Mg elemental distribution is also observed in the TMAZ and SZ, attributed to the formation

of Al-Mg phases. Copper (0.52 at%) manifests as discrete spots throughout the matrix, characteristic of its tendency to form intermetallic compounds, such as Al_2Cu and Al_4Cu_9, under the thermal conditions achieved at a TRS of 860 rpm, where the heat input is sufficient to promote intermetallic phase formation [18]. At the same time, the stirring action redistributes copper-rich phases to specific locations. Furthermore, the elemental distribution and precipitations on the nugget zone of FSW joints made at TRS of 1160 (Fig. 7) and 1460 rpm (Fig. 8) are not found adequately. The improper distribution of the elements would also be due to defects formed at higher TRS (Fig. 3 a, b).

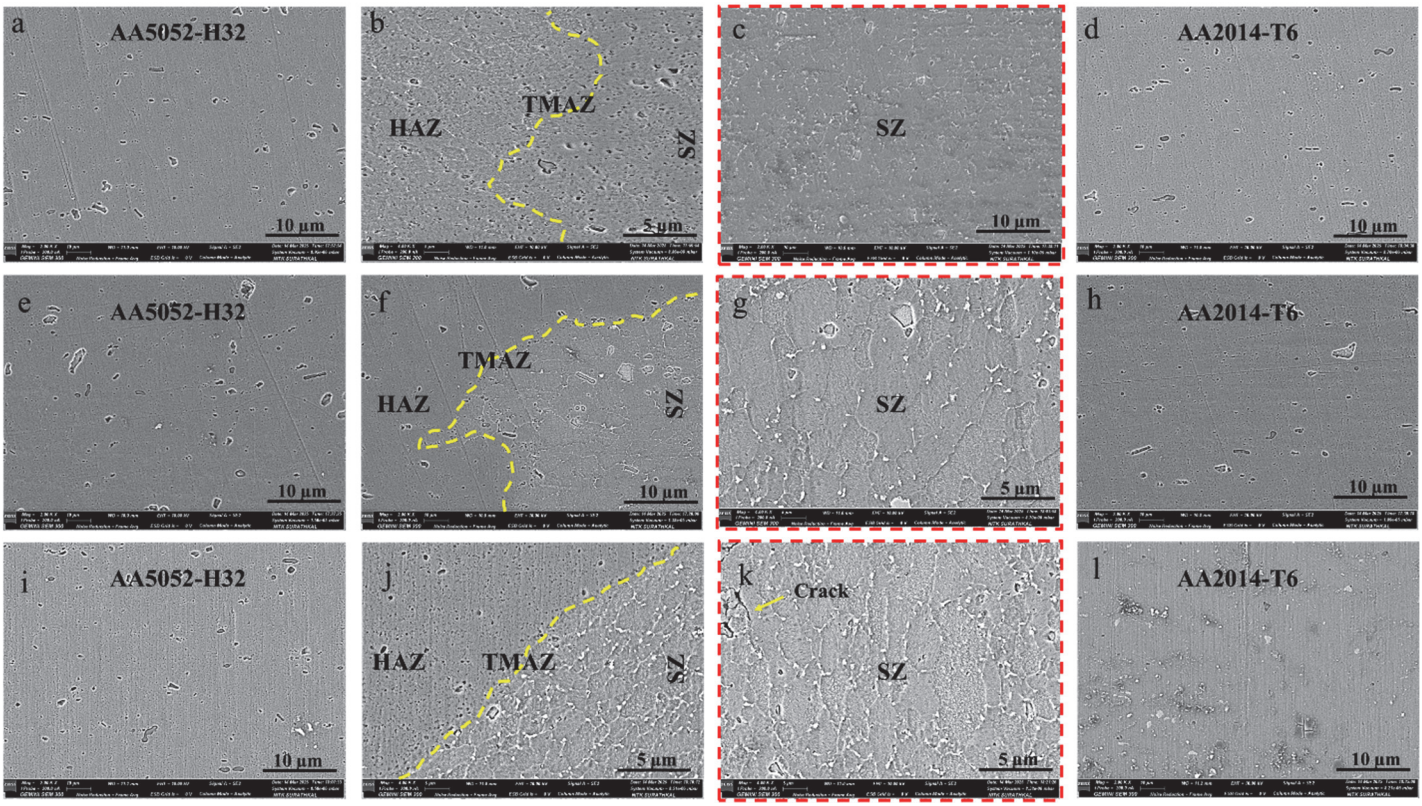

Figure 4: SEM images of various zones of FSW joints made at (a-d) 860 rpm, (e-h) 1160 rpm, and (i-l) 1460 rpm

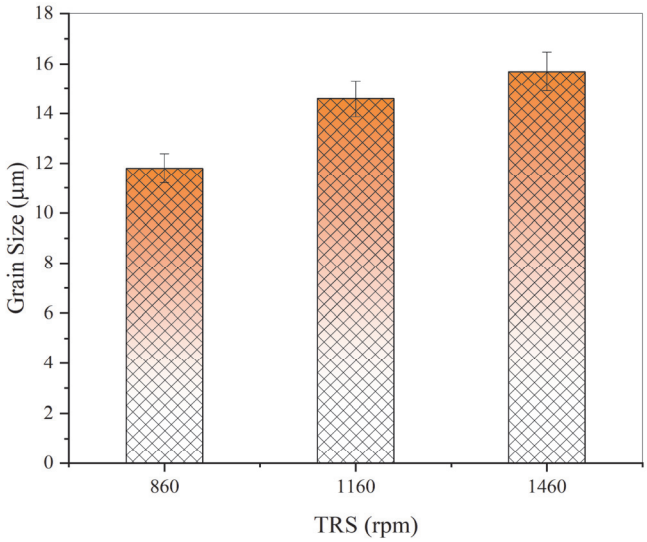

Figure 5: Grain size in the stir zone of FSW joints made with different TRS

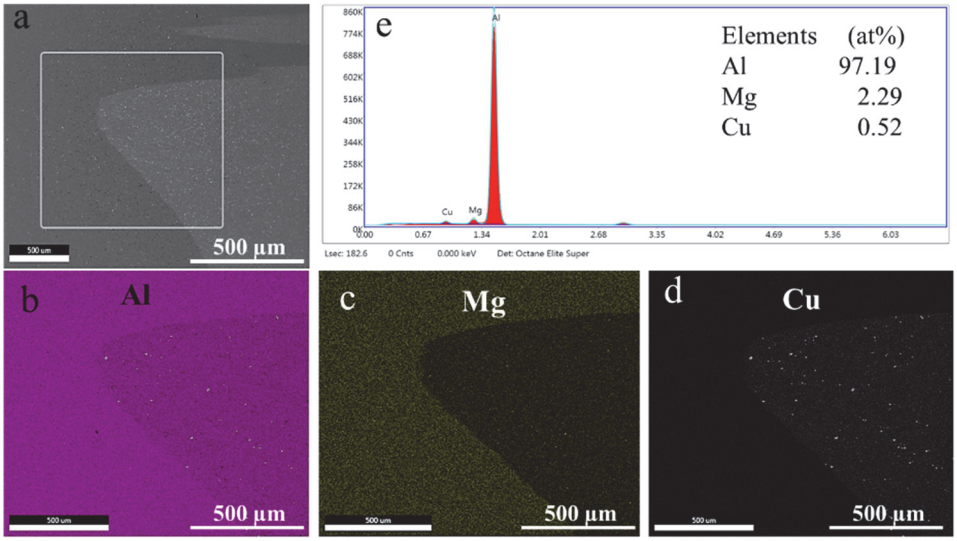

Figure 6: Elemental mapping of Al, Mg and Cu on the retreating side made at TRS of 860 rpm

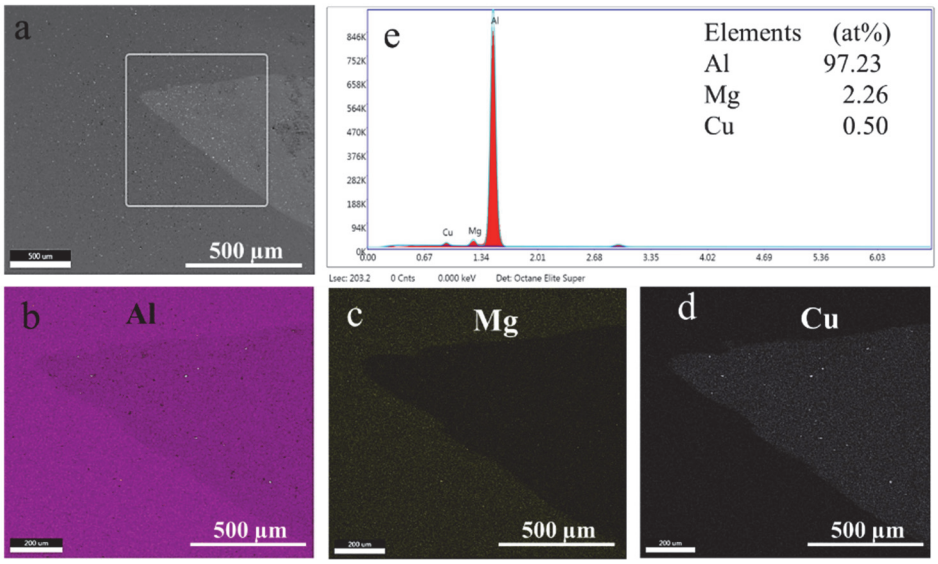

Figure 7: Elemental mapping of Al, Mg and Cu on the retreating side made at TRS of 1160 rpm

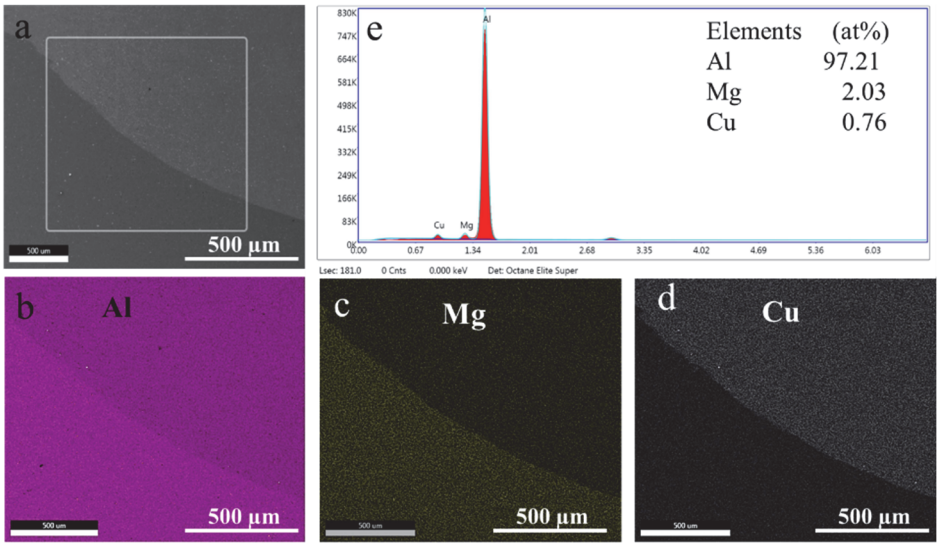

Figure 8: Elemental mapping of Al, Mg and Cu on the retreating side made at TRS of 1460 rpm

Hardness

Fig. 9 shows the schematic illustration of the indentation measurements across the weld section of the FSW joints. Fig. 10 shows the microhardness profile across the joint section of the FSW joints made at TRS of 860, 1160, and 1460 rpm. The SZ of all the FSW joints shows an increase in hardness compared to the other zones and base metal AA5052-H32. A maximum hardness of 156 ± 1.5 HV is observed at the joint made at 860 rpm TRS, which is almost near the hardness value of AA2014-T6 base metal. Further, the hardness decreased in the SZ with an increase in the TRS. This results from the increased coarsening of secondary phases at elevated temperatures caused by a rise in rotational speed [19]. Indentations at AA2014-T6 base metal show higher hardness compared to the SZ of higher TRS. The hardness profile of friction-stir welded joints of AA5052-H32 and AA2014-T6 dissimilar aluminium alloys exhibits a characteristic W-shaped distribution, which is directly associated with the complex microstructural evolution occurring across different zones. This observation is consistent with findings from several studies conducted on dissimilar aluminium alloys [15]. The drop in the hardness at higher TRS is also attributed to the defects formed in the nugget zone. The effect of TRS on the hardness behaviour is evident, as the 860-rpm condition produces the optimal hardness distribution with maximum stir zone strengthening and minimal HAZ softening. In contrast, higher rotation speeds result in progressive degradation of hardness due to excessive heat input, causing wider low-hardness zones and grain coarsening.

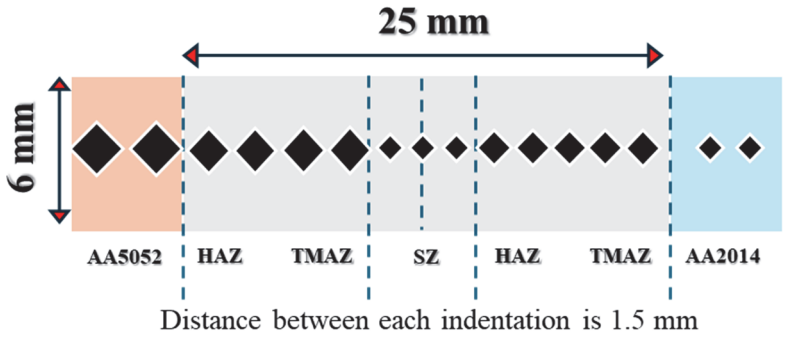

Figure 9: Schematic illustration of indentations across the weld section

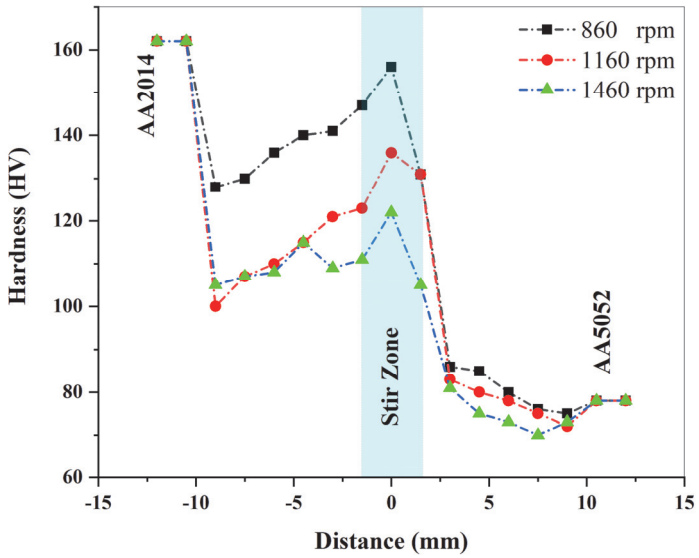

Figure 10: Hardness profile across the weld section of the FSW joints

Tensile behaviour of FSW joints

Fig. 11 (a, b) shows the tensile curves and UTS of the FSW joints made at various TRS. The results indicate a clear negative correlation between the TRS and UTS. A maximum UTS of 211 ± 1.0 MPa is observed at a rotational speed of 860 rpm, which subsequently decreases significantly to 189±2.1 MPa at 1160 rpm and further decreases to 172±1.5 MPa at 1460 rpm. From the photographic images of the tensile fractured specimens shown in Fig. 8 b, it is evident that the FSW joints made at TRS of 1160 and 1460 rpm failed near the weld line at HAZ of the weaker base material side, i.e., AA5052-H32. UTS decreases as the rotational speed increases, a phenomenon attributed to the heat generated during friction stir welding.

Tab. 4 illustrates the tensile properties of FSW joints. The yield stress, elongation, and the efficiency of the FSW joints decreased with an increase in TRS compared to the base metals. In the case of dissimilar alloys FSW, the tensile strength ratio of the FSW joint to any of the base materials is called joint efficiency. At lesser TRS, the heat input remains within the optimal range for these dissimilar aluminium alloys, promoting adequate plasticization and material mixing without excessive thermal exposure. A 93.8 % tensile strength of the base metal is achieved at the FSW joint made at TRS of 860 rpm. The progressive deterioration in tensile strength at higher rotation speeds can be attributed to excessive heat generation, which causes several metallurgical defects, including grain growth in the nugget zone, dissolution of strengthening precipitates, and the potential formation of brittle intermetallic compounds at the joint interface between the dissimilar alloys [20]. Additionally, the higher rotation speeds create turbulent material flow conditions that can lead to defect formation, such as voids, tunnelling, or wormhole porosity, due to insufficient material consolidation and irregular material transport around the tool pin [21]. The observed reduction in elongation from 16.1% at 860 rpm to 10.4% at 1460 rpm corroborates the decline in ductility as heat input increases, consistent with the transition from ductile to brittle fracture mechanisms under varying TRS conditions. Furthermore, the decrease in yield strength from 181±1.5 MPa to 155±2.0 MPa with increasing TRS emphasizes the critical importance of managing thermal exposure to maintain the weld strength properties. Excessive heat input leads to precipitate dissolution and softening effects, thereby compromising load-bearing capacity. As shown in Tab. 5, the trend of variation in tensile strength with variation of rotation speeds has been reported in numerous other research studies. The present study observed the highest ultimate tensile strength (UTS) at a TRS of 700 rpm, while a similar observation made by Rady et al. [22] reported a UTS of 199.819 MPa at a lower TRS. As the tool rotational speed increases, the resulting temperature rise gradually diminishes the ultimate mechanical strength of the weld assemblies.

Fracture Morphology

Fig. 12 (a-c) shows the SEM images of the failure locations of the FSW joints after the tensile test. The fractured surface produced at 860 rpm (Fig. 12 a) shows the micro-dimples and shallow dimples. The absence of voids, cracks, cleavage facets, and tear ridges stipulates a clear ductile fracture. It is also confirmed with the plastic behaviour shown in the tensile curve of the TRS at 860 rpm (Fig. 11). However, several circular and oval-shaped voids (inhomogeneous dimples), voids, and tear ridges were observed on the fractured surfaces at 1160 (Fig. 12 b) and 1460 rpm (Fig. 12 c). These features, which result from inadequate stirring, manifest at elevated rotational speeds. The occurrence of these defects is attributed to the temperature difference between the upper and lower sections, which interferes with the flow of material. Elevated rotational speeds result in higher temperatures and a slow cooling process within the stir zone. As illustrated in Fig. 11 (b), specimens welded at 860 rpm exhibited fracture away from the weld centerline on the retreating side, indicating failure at HAZ nearer to the AA5052-H32 base metal. Conversely, at 1160 rpm, the crack initiated in the heat-affected zone (HAZ) nearer to the stir zone, whereas at 1460 rpm, the fracture plane intersected the stir zone (SZ), mainly due to reduced hardness and grain coarsening. Moreover, high tool rotational speeds cause an irregular distribution of stirred material to the top surface, which both play a role in defect formation [25].

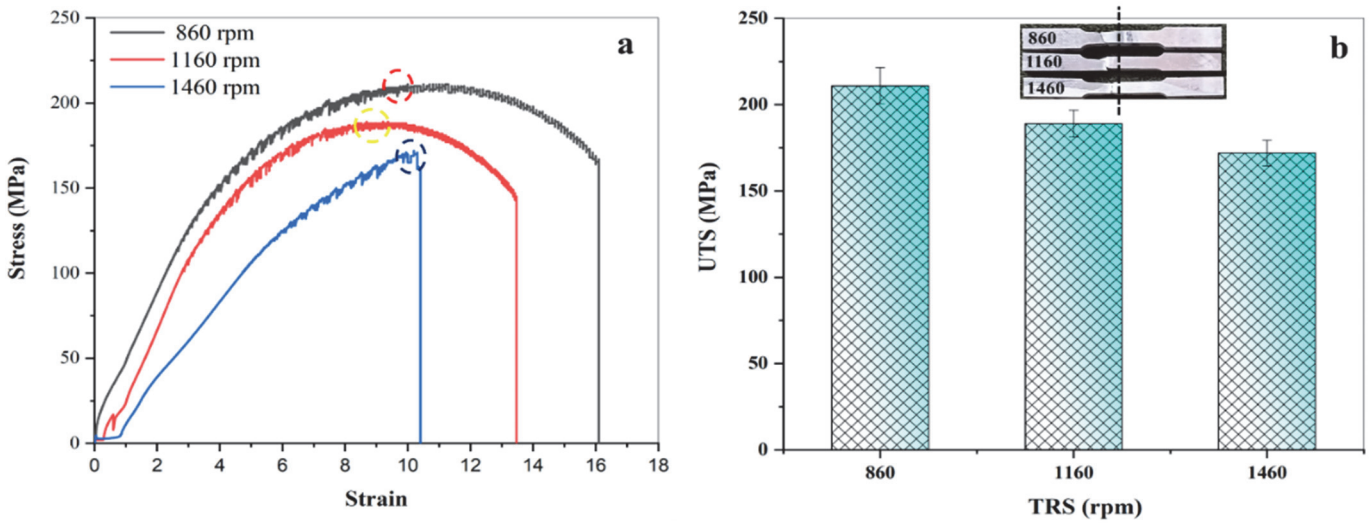

Figure 11: Tensile strength behaviour of the FSW joints a) stress vs strain curve, b) UTS vs TRS

Rotational speed(rpm)	0.2% Yield stress (MPa)	UTS (MPa)	Elongation (%)	Efficiency (%) in comparison to AA5052-H32 (225 MPa)
860	181±1.5	211±1.0	16.1	93.8
1160	168±2.0	189±2.1	13.5	84.0
1460	155±2.0	172±1.5	10.4	76.4

Table 4: Tensile properties of the FSW joints.

Base Metals Joined	Tool Rotation Speed (rpm)	UTS (trend)	Reference
AA6061/AA5083	700, 1050, 1400	↑ ↓ ↓	[22]
AA6061/AA5083	710, 900, 1120, 1400	↓ ↓ ↑ ↓	[23]
AA6082/AA6082	600, 800, 1000, 1200	↓ ↑ ↓ ↓	[10]

Table 5: Some of the studies that found a variation in UTS with a variation in TRS.

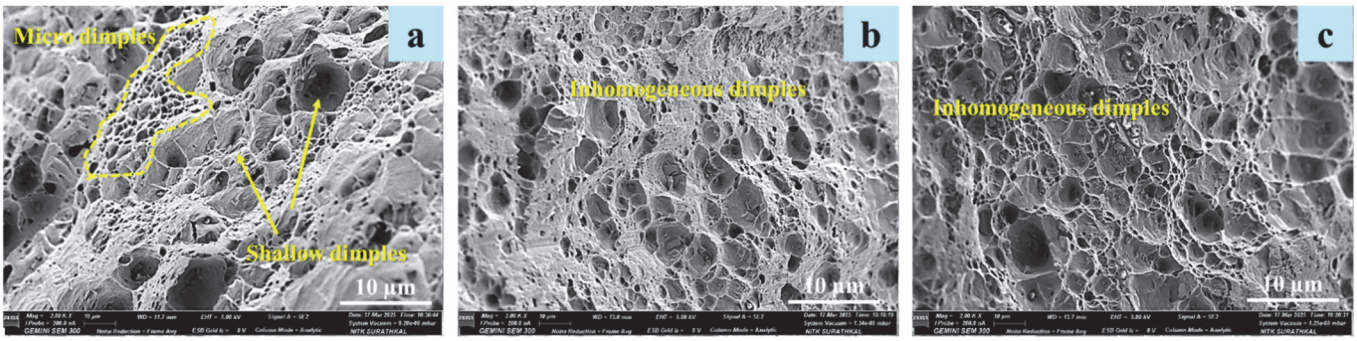

Figure 12: Fractured surfaces of the FSW joints made at a) 860 rpm, b) 1160 rpm, c) 1460 rpm

CONCLUSIONS

FSW of dissimilar aluminium alloys AA21014-T6 and AA5052-H32 is successfully obtained using various TRS in the range of 860-1460 rpm. The impact of tool rotation speed on the microstructure and mechanical properties is examined, and the following conclusions are drawn from this study.

- The weld surface morphology at 860 rpm exhibited a uniform, flash-free appearance with smooth, defect-free contours, indicating optimal material flow and consolidation achieved through balanced heat input and plastic deformation.
- The TRS of 860 rpm is observed with fine equiaxed grains (11.8 ± 0.3 µm), whereas higher TRS caused grain coarsening up to 15.7±0.5 µm
- A W-shaped hardness profile is observed across all joints, with maximum hardness of 156 ± 1.5 HV in the stir zone of the FSW joint made at 860 rpm
- Maximum UTS of 211 ± 1.0 MPa is achieved at the TRS of 860 rpm, demonstrating 93.8% efficiency compared to the base metal AA5052-H32.
- UTS has decreased with an increase in TRS due to the progressive deterioration of the weld region and excessive heat generation.
- Fractographic analysis revealed a ductile fracture characterized by micro-dimples at 860 rpm. The fracture type transitioned to a mixed-mode fracture exhibiting brittle characteristics at 1160 and 1460 rpm, which corresponds with decreased elongation and joint efficiency.

CONFLICTS OF INTEREST

The authors declare no conflict of interest

ACKNOWLEDGEMENT

The authors would like to thank CRF, NITK, Surathkal, for providing FSW welding and Testing facilities for this study.

REFERENCES

[1] Ahmed, M. M., El-Sayed Seleman, M. M., Fydrych, D., & Çam, G. (2023). Friction stir welding of aluminum in the aerospace industry: the current progress and state-of-the-art review. Materials, 16(8), 2971. DOI: https://doi.org/10.3390/ma16082971

[2] Balasubramanian, V. (2008). Relationship between base metal properties and friction stir welding process parameters. Materials Science and Engineering: A, 480(1-2), pp. 397-403. DOI: https://doi.org/10.1016/j.msea.2007.07.048.

[3] Singh, A., Sharma, S. K., Batish, A. (2025). Dynamic recrystallization during solid state friction stir welding/processing/additive manufacturing: Mechanisms, microstructure evolution, characterization, modeling techniques and challenges. Critical Reviews in Solid State and Materials Sciences, 50(1), pp. 77-135. DOI: https://doi.org/10.1080/10408436.2024.2391333.

[4] Nagaraja, S., Anand, P. B., Mariswamy, M., Alkahtani, M. Q., Islam, S., Khan, M. A., Bhutto, J. K. (2024). Friction stir welding of dissimilar Al–Mg alloys for aerospace applications: Prospects and future potential. Reviews on advanced materials science, 63(1), 20240033. DOI: https://doi.org/10.1515/rams-2024-0033.

[5] Ma, Z. Y., Feng, A. H., Chen, D. L., Shen, J. (2018). Recent advances in friction stir welding/processing of aluminum alloys: microstructural evolution and mechanical properties. Critical Reviews in Solid State and Materials Sciences, 43(4), pp. 269-333. DOI: https://doi.org/10.1080/10408436.2017.1358145.

[6] Routray, S., Swain, R., Mohapatro, R. N. (2025). Toward a Greener Weld for Integrating Sustainability Into Welding Practices. Advanced Welding Technologies, pp. 447-476. DOI: https://doi.org/10.1002/9781394331925.ch22

[7] Leon, J. S., Bharathiraja, G., & Jayakumar, V. (2020). A review on friction stir welding in aluminium alloys. In IOP conference series: materials science and engineering 954(1), 012007. DOI: https://doi.org/10.1088/1757-899X/954/1/012007.

[8] Dada, M., Popoola, P. (2024). Recent advances in joining technologies of aluminum alloys: a review. Discover Materials, 4(1), 86. DOI: https://doi.org/10.1007/s43939-024-00155-w.

[9] Thilagham, K. T., Noorullah, D. (2025). Effect of Tool Rotating Speed on Microstructure and Mechanical Properties of Dissimilar Friction Stir Welded AA5052-H32 and AA6082-T6 Aluminum Alloys. Journal of Materials Engineering and Performance, pp. 1-15. DOI: https://doi.org/10.1007/s11665-024-10017-4.

[10] Li, Y., Sun, D., Gong, W. (2019). Effect of tool rotational speed on the microstructure and mechanical properties of bobbin tool friction stir welded 6082-T6 aluminum alloy. Metals, 9(8), 894. DOI: https://doi.org/10.3390/met9080894.

[11] Kumar, S., Acharya, U., Sethi, D., Medhi, T., Roy, B. S., Saha, S. C. (2020). Effect of traverse speed on microstructure and mechanical properties of friction-stir-welded third-generation Al–Li alloy. Journal of the Brazilian Society of Mechanical Sciences and Engineering, 42(8), 423. DOI: https://doi.org/10.1007/s40430-020-02509-w.

[12] Venkatesh, B. N., Hebbal, U., Siddappa, P. N., Kousik, S., Nagaraja, T. K. (2022). Optimization of FSW parameters of AA6061-6 wt.% SiC composite plates. Manufacturing Review, 9, 34. DOI: https://doi.org/10.1051/mfreview/2022032.

[13] Ashok, S. K. (2023). A fuzzy model to predict the mechanical characteristics of friction stir welded joints of aluminum alloy AA2014-T6. The Aeronautical Journal, 127(1311), pp. 818-830. DOI: https://doi.org/10.1017/aer.2022.90.

[14] Li, J. Q., Liu, H. J. (2013). Effects of tool rotation speed on microstructures and mechanical properties of AA2219-T6 welded by the external non-rotational shoulder assisted friction stir welding. Materials & Design, 43, pp. 299-306. DOI: https://doi.org/10.1016/j.matdes.2012.07.011
[15] Gebreamlak, G., Palani, S., Sirahbizu, B. (2024). Mechanical characteristics of dissimilar friction stir welding processes of aluminium alloy [AA 2024-T351 and AA 7075-T651]. Manufacturing Review, 11, 19. DOI: https://doi.org/10.1051/mfreview/2024018
[16] Di Bella, G., Favaloro, F., Borsellino, C. (2023). Effect of process parameters on friction stir welded joints between dissimilar aluminum alloys: a review. Metals, 13(7), 1176. DOI: https://doi.org/10.3390/met13071176
[17] Nandan, R., DebRoy, T., Bhadeshia, H. K. D. H. (2008). Recent advances in friction-stir welding–process, weldment structure and properties. Progress in materials science, 53(6), pp. 980-1023. DOI: https://doi.org/10.1016/j.pmatsci.2008.05.001.
[18] Celik, S., Cakir, R. (2016). Effect of friction stir welding parameters on the mechanical and microstructure properties of the Al-Cu butt joint. Metals, 6(6), 133. DOI: https://doi.org/10.3390/met6060133.
[19] Zhang, C., Cao, Y., Huang, G., Zeng, Q., Zhu, Y., Huang, X., Liu, Q. (2020). Influence of tool rotational speed on local microstructure, mechanical and corrosion behavior of dissimilar AA2024/7075 joints fabricated by friction stir welding. Journal of Manufacturing Processes, 49, pp. 214-226. DOI: https://doi.org/10.1016/j.jmapro.2019.11.031.
[20] Saravana Sundar, A., Radhika, N., Kumar, A. (2024). Role of submerged friction stir welding in reducing intermetallic growth and enhancing microstructure in dissimilar Al-Ti joints. Scientific Reports, 14(1), 26908. DOI: https://doi.org/10.1038/s41598-024-78130-x.
[21] Zeng, X. H., Xue, P., Wang, D., Ni, D. R., Xiao, B. L., Wang, K. S., Ma, Z. Y. (2018). Material flow and void defect formation in friction stir welding of aluminium alloys. Science and Technology of Welding and joining, 23(8), pp. 677-686. DOI: https://doi.org/10.1080/13621718.2018.1471844.
[22] Rady, M. H., Khalafe, W. H., Jadoau, R. J., Kale, S. A., Shamsudin, S. (2024). Analysis of Tensile Strength of Friction Stir Welding for Aluminum Alloys AA6061 with AA5083 Using Design of Experiment Approach. Journal homepage: http://iieta. org/journals/ijcmem, 12(4), pp. 389-394. DOI: https://doi.org/10.18280/ijcmem.120407.
[23] Jha, S. K., & Prakash, P. (2023). Effect of tool rotation speed on mechanical properties of underwater friction stir welding of 6061-T6 and 5083-H12 aluminium alloys. Materials Today: Proceedings, 91, pp. 138-142. DOI: https://doi.org/10.1016/j.matpr.2023.03.753.
[24] Dialami, N., Cervera, M., & Chiumenti, M. (2020). Defect formation and material flow in friction stir welding. European Journal of Mechanics-A/Solids, 80, 103912. DOI: https://doi.org/10.1016/j.euromechsol.2019.103912.